Limit Load of Soil-Root Composites

Yang Pu[1], Xiang Zhihai[1], Hu Xiasong[2], Li Guorong[2], Zhu Haili[2]
Mao Xiaoqin[2] and Cen Zhangzhi[1,3]

Abstract: This paper studies the influence of root reinforcement on shallow soil protection by using Finite Element (FE) method. Taking the root-soil composite as a periodic material, the homogenization method is used to construct a Representative Volume Element (RVE) that consists of roots and soil. This RVE is discretized by a two-dimensional (2-D) FE mesh, while special formulation is established so that this model is capable of describing three-dimensional (3-D) deformations when the strain is invariant along the fiber axis. The important effect of debonding on the interface between the fiber and the matrix is also considered by using a special interface element. To verify the validity of the proposed computational model, triaxial tests were conducted, where the root-soil composite was subjected to axial and lateral pressures. Good agreement of limit loads has been achieved between the numerical and the experimental results.

Keywords: limit load, soil-root composites, soil-root interaction, periodic composites.

1   Introduction

In recent years, there has been increased awareness of the possibility of using vegetation to resist shallow landslide. This is especially important in *Qinghai-Tibet Plateau,* China, which is well-known by its adverse climatic conditions and the fragile ecological environment. In this region, the vegetation roots perform a very important role in improving shallow slope stability and reducing geological disasters. To improve the protection effect, it is important to study the mechanical properties of root-reinforced soil, especially the limit loads of soil-root composites.

Roots provide a reinforcing effect on the soil through their tensile resistance and pull-out resistance. The tensile strength of roots was measured to obtain the re-

[1] Department of Engineering Mechanics, Tsinghua University, Beijing 100084, P. R. China
[2] Department of Geological Engineering, Qinghai University, Xining 810016, P. R. China
[3] Corresponding author. Tel.: +86-10-62784015; E-mail: demczz@mail.tsinghua.edu.cn

lationship between root diameter and failure load [Wu et al. (1979); Nilaweera and Nutalaya (1999); Operstein and Frydman (2000)]. The pull-out tests were performed to measure friction between vertical roots and the soil [Nilaweera and Nutalaya(1999); Operstein and Frydman(2000)]. Direct shear tests of soils permeated by roots of vegetation have shown that roots can increase the strength of soil significantly. Laboratory shear tests of soil with roots [Waldon (1977)] and in situ shear tests on soil blocks with roots [Wu, Beal and Lan (1988)] were also conducted. These studies confirms that the shear strength can be increased by roots. In addition, a sort of analytical model of soil-root system was developed to analyze the soil-root interaction [Waldon (1977); Waldon and Dakessian (1981); Gray and Ohashi (1983); Wu, McOmber, Erb and Beal (1988)]. This kind of model was based on the Mohr-Coulomb equation and the soil shearing resistance was modified by a factor relating with root diameters.

The soil-root model can be considered as a kind of fiber-reinforced composite. Tremendous work has been devoted to the mathematical and numerical modeling of the behavior of composite materials in recent years. Early researches on composite materials were mainly based on the linear elastic model [Hashin and Rosen (1962); Hill(1965); Mori and Tanaka(1973)] and focused on the macroscopic descriptions according to empirical data. Most of these researches were later extended to predict the non-linear macroscopic behavior of composites. Pindera and Aboudi (1988) applied the method of cells to predict the initial yield surfaces of metal-matrix composites. Teply and Dvorak (1988) predicted the elastic-plastic response of composites reinforced by a periodic hexagonal array. Litewka (1980) presented experimental results of the overall plastic behavior of the perforated materials. With the rapid development of mathematical theory of homogenization in 1970s [Sahchez-Palencia (1980)], Suquet (1987) introduced the homogenization technique into classical elastic-plastic models for the study of composites at microscopic scale. Some valuable theoretical formulations were presented. Thereafter, the homogenization technique has been widely used in the study of composites. Based on this technique, the effective properties of composite materials with periodical microstructure were obtained by FE method [Michel, Moulinec and Suquet (1999)] and Fourier Transforms method [Michel, Moulinec and Suquet (2000)]. Okada, Fukui and Kumazawa (2004) also obtained the effective mechanical properties of particulate composite material by boundary element method. Carvelli, Maier and Taliercio (2000) applied the kinematic limit analysis to the RVE and obtained the limit loads of periodic materials. Buhan and Taliercio (1991) theoretically derived the macroscopic yield strength of a periodical composite. The prediction of the non-linear behavior of elastic-plastic composites subjected to a general state of stress has mostly been performed by using 3-D model, which leads to burdensome

numerical analyses. To solve this problem, Taliercio (2005) proposed an FE model to convert the 3-D analysis to the generalized plane strain analysis on any cross section of the composite.

One of the most significant characteristics of fiber-reinforced composites is the low strength of the interface between fibers and matrix [Benveniste (1985); Aboudi (1988)]. Aghdam, Smith and Pavier (2000) proposed initial yield and collapse load in fiber reinforced metal matrix composites with perfectly bonded or debonded interface on the basis of RVE. Han et al. (2006) studied the failure progression at the fiber-matrix interfaces in fiber-reinforced composite materials using a softening decohesion model. For the soil-structure interaction, a joint element was proposed on the basis of relative nodal displacement of solid elements surrounding the interface [Goodman, Taylor and Brekke (1968)]. A thin-layer element was proposed in soil-structure interaction and rock joints with a special constitutive model [Desai, Zaman, Lightner, Siriwardane (1984)].

In this paper, a soil-root composite RVE is established after the careful investigation of the root growth shape of vegetation in *Qinghai-Tibet Plateau*. The root growths unidirectional and arranges periodically, especially in cold and droughty area, so the homogenization technique can be introduced to analyze the soil-root composites. In Section 2 some basic concepts are briefly reviewed regarding the theory of homogenization. To reduce computational burden, the 2-D FE model of soil-root composites, which is capable of describing 3-D deformations, is established based on RVE. In this new type of 2-D FE, the displacement field is subdivided into average and fluctuation parts and the periodical boundary condition is applied to the fluctuation part directly. Considering the low strength of the interface between fiber and matrix, the Goodman element is introduced to the RVE and is modified to satisfy the periodic condition. In Section 3, the soil-root composites are studied according to experimental method. A kind of vegetation named *Elymus dahuricus Turcz* is selected as the specimen, which is a popular vegetation to decrease shallow landslide and protect soils in *Qinghai-Tibet Plateau*. The elastic properties and yield strength of root and soil are obtained through basic material experiments. From the in situ investigation, the root fraction is between 0.5% and 1%. Accordingly, two soil-root composite specimens with the root fraction of 0.5% and 1%, respectively, were subjected to three-axial loads. The experimental data obviously show the reinforcement of the root and the effect of the interface. In addition, the FE models with the same fiber fraction are established to simulate the experiments of soil-root composites. The obtained numerical limit loads are in good agreement with experimental results.

2   The numerical formulation of soil-root RVE

2.1   Homogenization theory for periodical composites

Homogenization is the substitution of real heterogeneous composites with an ideal, homogeneous continuum. The properties of this composite structure are derived through analyses of a RVE. If the heterogeneous composites consist of a matrix embedding uniformly distributed inclusions of the same shape, the composite structure is said to be periodical, and a single unit cell can be taken as a RVE. The model of periodical composites is shown in Figure 1. To determine the effective properties of a composite, two well separated scales are established. A local scale (x) is small enough to describe microstructure and an overall scale (y) is large enough to consider the RVE as a macroscopic point of the composites.
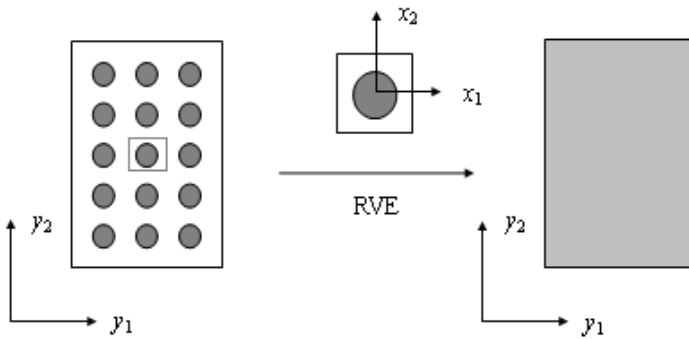
Figure 1: Periodical microstructures and a RVE of a composite

To characterize the overall properties of the composite, overall stress Σ and overall strain E are defined as the average over any RVE of the corresponding local quantities, σ and ε.

$$\Sigma = \langle \sigma \rangle = \frac{1}{V} \int_V \sigma dV$$
$$E = \langle \varepsilon \rangle = \frac{1}{V} \int_V \varepsilon dV \tag{1}$$

Here, V is the volume of the periodical RVE, $\langle \cdot \rangle$ stands for the averaging operator.

In periodical composites, the local mechanical fields in the RVE can be divided into the overall average term and the local fluctuation term and admit the following

decomposition:

$$u = E \cdot x + \tilde{u}$$
$$\varepsilon = E + \tilde{\varepsilon} \qquad (2)$$
$$\sigma = \Sigma + \tilde{\sigma}$$

Here, u, ε and σ denote the local displacement, strain and stress field, respectively; $\tilde{u}$, $\tilde{\varepsilon}$ and $\tilde{\sigma}$ are their fluctuation terms, and $\tilde{u}$ are periodical on the boundary of the RVE.

The overall quantities Σ and E should satisfy the Hill's lemma:

$$\langle \sigma : \varepsilon \rangle = \Sigma : E. \qquad (3)$$

This equation is the basis of energy approaches to evaluate bounds to the yield strength of fiber reinforced composites.

2.2 Numerical discritization by 2-D FE for generalized plane strain problems

The appropriate kinematic assumption for the analysis of any RVE of a composite reinforced by an array of long, parallel fibers is that the RVE is in the state of *generalized plane strain* (GPS). This assumption requires the displacement and strain to satisfy:

1. the strain is invariant along the fiber axis.

2. the displacement must be, at most, linear in fiber axis.

3. the axial strain is necessarily constant through the RVE.

A 2-D FE with $n^{(e)}$ nodes is constructed based on the above assumptions. Each node has three Degrees of Freedom (DOF), corresponding to the components of the nodal fluctuation displacement $\tilde{U}_j^{(e)} = \left\{ \tilde{u}_j^{(e)}, \tilde{v}_j^{(e)}, \tilde{w}_j^{(e)} \right\}^{\mathrm{T}}$, $j = 1 \cdots n^{(e)}$. Each component of the displacement field $u = \{u, v, w\}^{\mathrm{T}}$, is discretized in the following form:

$$
\begin{aligned}
u^{(e)}(x,y) &= E \cdot x(x,y) + \tilde{u}^{(e)}(x,y) \\
&= E \cdot x(x,y) + N^{(e)}(x,y) \tilde{U}^{(e)}(x,y),
\end{aligned} \qquad (4)
$$

where $\tilde{U}^{(e)}$ is $3 \times n^{(e)}$ nodal DOF and E is 3×3 overall strain matrix. $N^{(e)}$ is the in-plane shape function matrix for $n^{(e)}$-node 2-D element.

The fluctuation strain $\tilde{\varepsilon} = \{\tilde{\varepsilon}_x, \tilde{\varepsilon}_y, \tilde{\varepsilon}_z, \tilde{\gamma}_{xy}, \tilde{\gamma}_{xz}, \tilde{\gamma}_{yz}\}^{\mathrm{T}}$ is discretized as:

$$\tilde{\varepsilon}^{(e)}(x,y) = B^{(e)}(x,y)\tilde{U}^{(e)}(x,y). \tag{5}$$

Here, $B^{(e)}$ is the in-plane compatibility matrix, which can be split into 6×3 sub-matrices, $B_j^{(e)}, j = 1 \cdots n^e$. Each $B_j^{(e)}$ is given by

$$B_j^{(e)} = \begin{bmatrix} \frac{\partial N_j^{(e)}}{\partial x} & 0 & 0 \\ 0 & \frac{\partial N_j^{(e)}}{\partial y} & 0 \\ 0 & 0 & 0 \\ \frac{\partial N_j^{(e)}}{\partial y} & \frac{\partial N_j^{(e)}}{\partial x} & 0 \\ 0 & 0 & \frac{\partial N_j^{(e)}}{\partial x} \\ 0 & 0 & \frac{\partial N_j^{(e)}}{\partial y} \end{bmatrix}, \quad j = 1 \cdots n^e. \tag{6}$$

The discretized form of Eq.(3) reads as [Michel, Moulinec and Suquet (1999)]

$$\begin{bmatrix} K & \bar{K} \\ \bar{K}^{\mathrm{T}} & \bar{\bar{K}} \end{bmatrix} \begin{Bmatrix} \tilde{U} \\ E \end{Bmatrix} = \begin{Bmatrix} 0 \\ \Sigma \end{Bmatrix}. \tag{7}$$

Here, the stiffness matrix reads:

$$\begin{aligned}
K &= \sum_e k^{(e)}, \\
k^{(e)} &= \frac{1}{V} \int_e B^{(e)\mathrm{T}} D^{(e)} B^{(e)} dV \\
\bar{K} &= \sum_e \bar{k}^{(e)}, \\
\bar{k}^{(e)} &= \frac{1}{V} \int_e B^{(e)\mathrm{T}} D^{(e)} dV \\
\bar{\bar{K}} &= \sum_e \bar{\bar{k}}^{(e)}, \\
\bar{\bar{k}}^{(e)} &= \frac{1}{V} \int_e D^{(e)} dV
\end{aligned} \tag{8}$$

Considering the periodicity of RVE, the fluctuation displacement $\tilde{u}$ must satisfy periodic boundary conditions:

$$\tilde{u}_A = \tilde{u}_B, \tag{9}$$
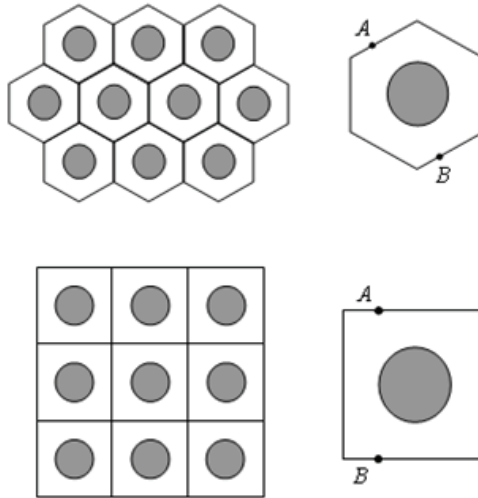
Figure 2: Periodicity boundary conditions

where, (A, B) is any pair of nodes on any side of the RVE, symmetrical with respect to the symmetrical axial of the RVE. In Figure 2, the symmetrical nodes are denoted in square and hexagonal array RVEs.

The periodical boundary conditions must be considered as constrains imposed to the discrete FE equation, Eq.(7).

2.3 FE formulation with debonded interface element

In the simulation of soil-root composite, the low strength of the interface must be considered. For this purpose, the Goodman interface element is modified to satisfy the periodic condition.

Two sets of Cartesian coordinates are established. One is the global coordinates $OXYZ$, where the displacement is u and the fluctuation displacement is $\tilde{u}$; the other is local coordinates $O'X'Y'Z'$, where the displacement is u' and the fluctuation displacement is $\tilde{u}'$. The transformation matrix between these two coordinates is denoted as the matrix T.

$$u' = Tu$$
$$\tilde{u}' = T\tilde{u} \tag{10}$$

The constructed interface element with $m^{(e)}$ nodes is shown in Figure 3. For the interface element in GPS state, the 2-D interface element can also describe 3-D

failure mode. In local coordinates $O'X'Y'Z'$, each node has three DOF $U'^{(e)}_j = \left\{u'^{(e)}_j, v'^{(e)}_j, w'^{(e)}_j\right\}^{\mathrm{T}}$, $j = 1 \cdots m^{(e)}$, and the corresponding fluctuation displacements are $\tilde{U}'^{(e)}_j = \left\{\tilde{u}'^{(e)}_j, \tilde{v}'^{(e)}_j, \tilde{w}'^{(e)}_j\right\}^{\mathrm{T}}$, $j = 1 \cdots m^{(e)}$.
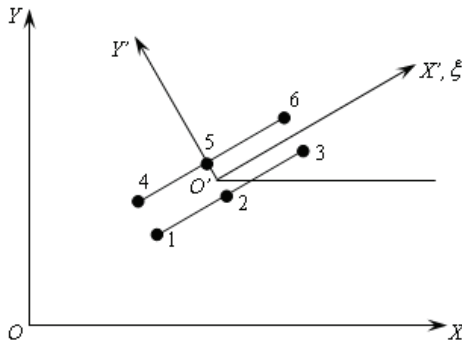
Figure 3: Six-node interface element

The displacement field can be discretized in the following form:

$$
\begin{aligned}
u'^{(e)}_{upper} &= N^{(e)} U'^{(e)}_{upper} \\
u'^{(e)}_{lower} &= N^{(e)} U'^{(e)}_{lower}
\end{aligned}
\tag{11}
$$

Here, $u'^{(e)}_{upper}$ and $u'^{(e)}_{lower}$ are the displacements in the upper edge and the lower edge of the interface element, respectively. $U'^{(e)}_{upper}$ and $U'^{(e)}_{lower}$ are the corresponding nodal displacement vector. The corresponding discretization form of the fluctuation displacement field is given by

$$
\begin{aligned}
\tilde{u}'^{(e)}_{upper} &= N^{(e)} \tilde{U}'^{(e)}_{upper} \\
\tilde{u}'^{(e)}_{lower} &= N^{(e)} \tilde{U}'^{(e)}_{lower}
\end{aligned}
\tag{12}
$$

where $N^{(e)}$ is the shape function in one dimension, which can be split into 3×3 sub-matrices, each one pertinent to one node:

$$
N_j(x') = N_j(x') \begin{bmatrix} 1 & 0 & 0 \\ 0 & 1 & 0 \\ 0 & 0 & 1 \end{bmatrix}, \quad j = 1 \cdots \frac{m^{(e)}}{2};
\tag{13}
$$

Because in this interface element, one point on the upper edge requires a paired point on the lower edge, the total number of element nodes $m^{(e)}$ must be even. The difference of the displacement between upper and lower edge is given by

$$\Delta u'^{(e)} = N^{(e)} \left(U'^{(e)}_{upper} - U'^{(e)}_{lower} \right). \tag{14}$$

Considering the thickness of the interface element t is much smaller than the dimension of the adjacent element, the difference of the overall displacement can be ignored. The difference of the fluctuation displacement can be read as

$$\begin{aligned}
\Delta u'^{(e)} &= \Delta \tilde{u}'^{(e)} \\
&= N^{(e)} \left(\tilde{U}'^{(e)}_{upper} - \tilde{U}'^{(e)}_{lower} \right) \\
&= \begin{bmatrix} -N^{(e)} & \\ & N^{(e)} \end{bmatrix} \begin{bmatrix} \tilde{U}'^{(e)}_{lower} \\ \tilde{U}'^{(e)}_{upper} \end{bmatrix} \\
&= \begin{bmatrix} -N^{(e)} & \\ & N^{(e)} \end{bmatrix} \tilde{U}'^{(e)} \\
&= \begin{bmatrix} -N^{(e)} & \\ & N^{(e)} \end{bmatrix} T^{(e)} \tilde{U}^{(e)}
\end{aligned} \tag{15}$$

Supposing the thickness of the interface element t is constant and the strain of the interface element is

$$\varepsilon'^{(e)} = \left\{ \begin{array}{c} \gamma'^{(e)}_{X'Y'} \\ \varepsilon'^{(e)}_{Y'} \\ \gamma'^{(e)}_{Y'Z'} \end{array} \right\} = \frac{1}{t} \left\{ \begin{array}{c} \Delta u'^{(e)}_{X'Y'} \\ \Delta u'^{(e)}_{Y'} \\ \Delta u'^{(e)}_{Y'Z'} \end{array} \right\} = \frac{1}{t} M^{(e)} \tilde{U}'^{(e)} = \frac{1}{t} M^{(e)} T^{(e)} \tilde{U}'^{(e)}, \tag{16}$$

where, $M^{(e)}$ is given by

$$M^{(e)} = \begin{bmatrix} -N^{(e)}_1 & \cdots & -N^{(e)}_{\frac{m^{(e)}}{2}} & N^{(e)}_1 & \cdots & N^{(e)}_{\frac{m^{(e)}}{2}} \end{bmatrix}. \tag{17}$$

The compatibility matrix in interface element reads

$$B^{(e)} = \frac{1}{t} M^{(e)}. \tag{18}$$

From the Hill's lemma (Eq. (3)), the discretized FE equation for the RVE with debonded interface has the same form as Eq. (7), while the stiffness matrix is

modified as follows:

$$K = \sum_{e,stru} k_1^{(e)} + \sum_{e,inter} k_2^{(e)},$$

$$k_1^{(e)} = \frac{1}{V} \int_e B^{(e)^{\mathrm{T}}} D^{(e)} B^{(e)} dV$$

$$k_2^{(e)} = \frac{1}{V} \int_e T^{(e)^{\mathrm{T}}} B^{(e)^{\mathrm{T}}} D^{(e)} B^{(e)} T^{(e)} dV$$

$$\bar{K} = \sum_{e,stru} \bar{k}^{(e)}, \tag{19}$$

$$\bar{k}^{(e)} = \frac{1}{V} \int_e B^{(e)^{\mathrm{T}}} D^{(e)} dV$$

$$\bar{\bar{K}} = \sum_{e,stru} \bar{\bar{k}}^{(e)},$$

$$\bar{\bar{k}}^{(e)} = \frac{1}{V} \int_e D^{(e)} dV$$

Here, the elastic matrix $D^{(e)}$ on the interface is given by

$$D^{(e)} = \begin{bmatrix} K_{X'Y'} & 0 & 0 \\ 0 & K_{Y'} & 0 \\ 0 & 0 & K_{Y'Z'} \end{bmatrix}, \tag{20}$$

where

$$K_{X'Y'} = K_{Y'Z'} = \frac{E}{2(1+v)}$$

$$K_{Y'} = \frac{E(1+v)}{(1+v)(1-2v)} \tag{21}$$

E is the elastic modulus and v is the Poisson's ratio. The stress $\sigma'^{(e)}$ in the interface reads as

$$\sigma'^{(e)} = \begin{Bmatrix} \tau'^{(e)}_{X'Y'} \\ \sigma'^{(e)}_{Y'} \\ \tau'^{(e)}_{Y'Z'} \end{Bmatrix} = \begin{bmatrix} K_{X'Y'} & 0 & 0 \\ 0 & K_{Y'} & 0 \\ 0 & 0 & K_{Y'Z'} \end{bmatrix} \begin{Bmatrix} \gamma'^{(e)}_{X'Y'} \\ \varepsilon'^{(e)}_{Y'} \\ \gamma'^{(e)}_{Y'Z'} \end{Bmatrix}. \tag{22}$$

The parameters in elastic matrices $K_{X'Y'}$, $K_{Y'Z'}$ and $K_{Y'}$ must be adjusted to represent two major failure modes of the interface, i.e., the slip and debonding. Here, the interface stress $\sigma'^{(e)}$ is used in the interface criteria for this purpose.

When $\sigma'^{(e)}_{Y'} \leq \sigma'_{cri}$, the interface is in stick or rebonding mode. The elastic matrix can be formed according to Eq. (21).

When $\sigma'^{(e)}_{Y'} > \sigma'_{cri}$, the interface is in debonding mode. The elastic constant should equal to zero. To avoid the numerical singularity, the elastic constants $K_{X'Y'}$, $K_{Y'Z'}$ and $K_{Y'}$ can also be set as small values.

When $\tau'^{(e)}_{X'Y'} > \tau'_{cri}$ or $\tau'^{(e)}_{Y'Z'} > \tau'_{cri}$, the interface is in slip mode. The corresponding parameters $K_{X'Y'}$ and $K_{Y'Z'}$ should be replaced by zeroes or small values. The slip mode can only occur when the normal stress $\sigma'^{(e)}_{Y'}$ is compressive.

σ'_{cri} and τ'_{cri} are the critical stresses which are determined by the material model used. Mohr-Coulomb criteria

$$\tau'_{cri} = c + \sigma^{(e)}_{Y'} \tan \varphi. \tag{23}$$

are mostly used to define the initiation of slip for the soil-structure interface. Here, c and φ are the cohesion and friction angle of the soil. For the perfectly strong interface, σ'_{cri} and τ'_{cri} can choose large values. The interface will never break. For the perfectly weak interface, σ'_{cri} and τ'_{cri} can both equal to zero. The interface is therefore only able to transfer compression force.

3 Experimental study of the soil-root composites

Qinghai-Tibet Plateau is called the Asia's water tower. The vegetation is much useful to reserve water and protect soil. The experiments of soil-root composites were carried out in Xining, Qinghai Province, China. The *Elymus dahuricus Turcz,* a popular vegetation to prevent shallow landslide and protect soils in *Qinghai-Tibet Plateau*, was selected to study the strength of the soil-root composites. In this section, the basic material parameters were obtained for the numerical simulation. The triaxial tests were performed to study the root reinforcement to the soil.

3.1 Material parameters of root and soil

Tension tests were carried out to obtain the material parameters of the *Elymus dahuricus turcz* roots. The obtained elastic modulus was 101.9257MPa, and yield stress was 50.7739MPa.

The soil was obtained from the North Mountain in Xining. The big soil grains were eliminated through the sieve with 2mm pores. From triaxial tests the obtained elastic modulus was 0.001168MPa; the cohesion was 0.009556MPa; and the angle of friction was 24.716 degree.

The natural soil-root composites, shaped in a cylinder with 120mm in height and 61.8mm in diameter, were also obtained from the North Mountain. The roots collected from the smashed natural composites weighted about 1.847g. The weight of a single root with 120mm in height and 0.4mm in diameter was about 0.011g.

The total number of roots was 168. In the following triaxial tests, the man-made specimens were in the same dimension with the same number of roots.

3.2 The triaxial test of soil-root composites

The triaxial test is commonly used to obtain the strength parameters of soil. To prove the reinforcement of the root, the soil-root composites were subjected to the triaxial test.

The specimen of the soil-root composite was shaped in a cylinder. The roots were aligned in parallel along the axis of the specimen. The arrangement of the roots was homogeneous and periodical, which is shown in Figure 4.
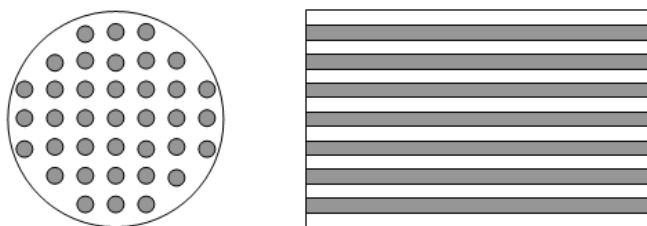
Figure 4: The arrangement of roots in composites

To simulate the natural state, the root fraction of the specimen was close to natural root fraction. Two sets of specimens of 0.5% and 1% root fractions were prepared. The diameter of each root was measured and the total area of roots in one specimen was ensured to be 0.5% or 1%.

To facilitate the preparation of the specimen, the soil and roots were provided independently in advance. All the roots, measured one by one, were 12mm in length and approximately had the same diameter of the cross section. The number of roots was determined by the total cross-sectional area of all the roots, which was equal to 0.5% or 1% of the cross-sectional area of the specimen. In general triaxial tests of pure soil, the same compactness of a series of specimen was ensured by the same tamped method by hammer. The same weight of soil was used to assure the same compactness in the triaxial test of soil-root composites. The pure soil specimen in Section 3.1 was weighed, which is denoted by m_{soil}. Then the soil, whose weight was $0.995m_{soil}$ or $0.99m_{soil}$, was used for the preparation of the specimen with different fiber fraction.

The specimen was made in a columniform metal box. Two thirds of the box laid on the ground flatways. A layer of soil was placed in the box and a layer of roots

was placed on the soil along the axial of the cylinder immediately. The soil and the roots were put into the box alternately in this way and stopped when 90% of the soil and all the roots were filled into the box. The remainder one third of the box was placed on the specimen to form a whole columniform box and tamp the composites. The specimen was tamped by hammer after the remainder soil was placed to the two ends of the mental box. The specimen and the root arrangement in composites are shown in Figure 5 and Figure 6.

Figure 5: Specimen of composites

The specimen was subjected to the triaxial test. The lateral pressure of 0.01MPa was kept through the whole test process. The axial pressure was gradually increased until the failure of the specimen appeared. The failure mode is shown in Figure 7.

The results of the triaxial tests on soil-root composites with different fiber fraction are listed in Table 1 and Table 2.

The limit load of axial pressure in pure soil specimen was 0.0543MPa, which was obtained according to general soil mechanics experiment in Section 3.1. Obvious reinforcement effect of roots can be proved by comparing the limit load of pure soil specimen with the average axial limit loads listed in Table 1 and Table 2.

Figure 6: Root arrangement in composites

Table 1: Experiment result of soil-root composites with 0.5% fiber fraction

	Number of roots	Average diameter of roots (mm)	Axial limit pressure (MPa)
Sample 1	128	0.385	0.07740
Sample 2	142	0.365	0.08176
Sample 3	123	0.392	0.06978
Sample 4	127	0.387	0.06006
Average			0.07225

Table 2: Experiment result of soil-root composites with 1% fiber fraction

	Number of roots	Average diameter of roots (mm)	Axial limit pressure (MPa)
Sample 1	245	0.393	0.08105
Sample 2	249	0.391	0.08640
Sample 3	244	0.394	0.09301
Average			0.08682

Fiber fraction=0.5%

Fiber fraction=1%

Figure 7: The failure mode of soil-root composites

4   Numerical Examples

4.1   *Limit loads of metal matrix composites*

These composites consist of a titanium matrix IMI 318, which is reinforced by continuously aligned silicon carbide fibers (SM 1240) with volume fraction 35%. Elastic perfectly plastic properties are used for the matrix in the FE model. For the IMI 318 matrix, the elastic modulus is 107 GPa; Poisson's ratio is 0.3 and the yield stress is 940 MPa. The SM1240 fiber is assumed to be isotropic and linear elastic with elastic modulus of 409 GPa and Possion's ratio of 0.2. 8-node elements presented in Section 2.2 and 6-node interface element in Section 2.3 are used to discretize the RVE. Periodical boundary condition is applied to the RVE. The FE mesh is shown in Figure 8.
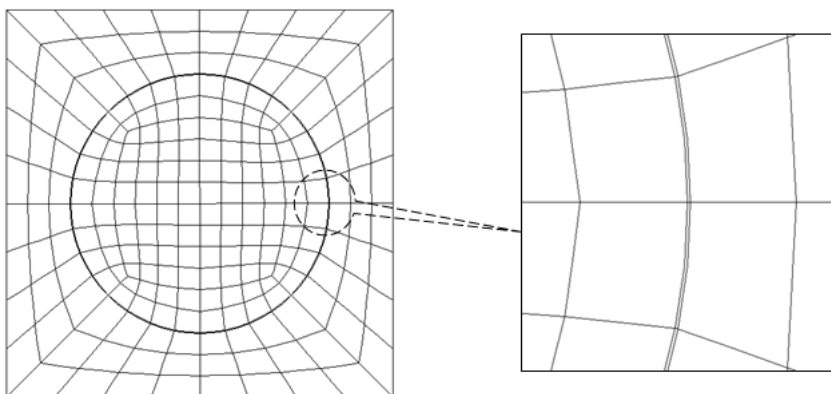
Figure 8: Finite element mesh of RVE with 35% fiber fraction

A perfectly strong and a perfectly weak interface model are used to determine the failure mode of the interface. In perfectly strong interface model, the interface does not slip during the whole loading process. While in perfectly weak interface model, the interface is only able to transfer compression force between fibers and matrix, ignoring the friction. These two models can be considered to be the two extreme behaviors of the actual material.

The FE model is subjected to transverse stresses. The obtained limit loads are compared with Aghdam's results [Aghdam, Smith and Pavier (2000)] in Table 3.

Table 3: Limit loads of the metal matrix composites in transverse load

	Bonded interface(MPa)		Debonded interface(MPa)	
	Limit load	Aghdam's	Limit load	Aghdam's
Uniaxial tension	1.20	1.16	0.47	0.48
uniaxial compression	-1.20	-1.16	-0.87	-0.87

4.2 Limit loads of soil-root composites in triaxial tests

The triaxial test performed in Section 3.2 is simulated according to the RVE method presented in Section 2. Two RVEs with fiber fraction of 0.5% and 1% are established. Material parameters of the soil and roots were obtained from the experiments performed in Section 3.1. The elastic modulus of soil is 0.001168MPa, the Possion's ratio is assumed to be 0.2. The soil matrix satisfies Drucker-Prager criterion with circumcircle assumption. The cohesion is 0.009556MPa, and the angle of friction is 24.716 degree. The elastic modulus of roots is 101.805MPa and the Poisson's ratio is assumed to be 0.3. The root satisfies von Mises criterion. The yield stress is 50.7739MPa. 8-node elements and 6-node interface elements are used to discretize the RVE.

On the interface, only compression force can be transferred. So when the normal stress in interface elements is greater than zero, the interface fails. The friction between fibers and matrix is considered. Mohr-Coulomb criterion (Eq. (23)) is used to determine the critical shear stress. The material parameters in Eq. (23) are the same as the soil matrix. The composite fails when the whole interface is debonded or the incremental load is very small. The corresponding load is the limit load.

Periodic boundary condition is applied to the RVE. The FE mesh is shown in Figure 9.

The loading process is the same as the experiment. With lateral pressure of 0.01MPa, the soil-root composites are subjected to the axial pressure step by step. When all the interface elements are debonded, the soil-root composite is destroyed and the limit load is obtained. The limit loads of axial pressure in different fiber fraction are listed in Table 4.

Table 4: Limit loads of axial pressure in triaxial tests

Fiber fraction	Numerical result (MPa)	Experimental data (MPa)
0.5%	0.0839	0.07225
1%	0.1130	0.08682
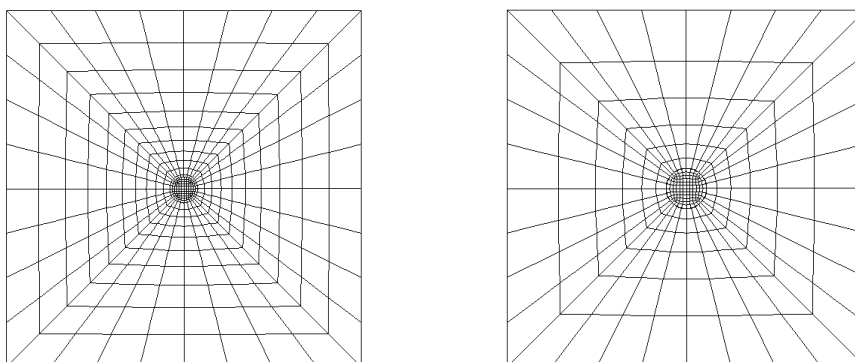
Fiber fraction = 0.5%   Fiber fraction = 1%

Figure 9: FE mesh of RVE with fiber fraction of 0.5% and 1%

In Table 4, the numerical solution is greater than the experimental data. This is mainly due to the difficulty of preparing the specimen of soil-root composites and the circumcircle Drucker-Prager yield criterion.

In Section 3.2, because the roots were arranged in the soil by hand and the roots were not very straight, it was difficult to arrange the roots homogeneously. Though the fiber fraction is 0.5% or 1% in average, there must be some parts of the soil-root composites, whose fiber fraction are less than 0.5% or 1%. These unhomogeneity would decrease the strength of the composites. The difficulty of homogeneous arrangement in 1% fraction is greater than that of 0.5% in the same columniform box. So from the numerical and experimental results, the error of the result with 1% fiber fraction is lager than that of 0.5%. In addition, the circumcircle Druker-Prager yield criterion is used in the composites RVE model. It is reasonable that the numerical result is greater than the real value. However, the computational solution becomes larger with the increase of the fiber fraction. It proves that the strength of soil is reinforced by roots.

4.3   In-plane limit loads of soil-root composites

The soil-root RVE subjected to uniaxial in-plane loads are simulated in this section. The FE model and material parameters are the same as the model in Section 4.2. The numerical solutions of limit loads are listed in Table 5.

From Table 5, the reinforcement of the root is almost the same in tensile and compression loads. In uniaxial tension and uniaxial compression, the reinforcement of

Table 5: Limit loads of soil-root composites with different fiber fraction

	Limit load (MPa) (fiber fraction=0.5%)	Limit load (MPa) (fiber fraction=1%)
Uniaxial tension	0.0154	0.0140
Uniaxial compression	-0.0599	-0.0590

the root fiber can be ignored because of weak interfaces. The soil matrix mainly bears the in-plane loads. So the limit loads even decrease a little with the increase of the fiber fraction.

5 Discussion

In this paper, a 2-D FE of composite RVE is established based on homogenization method. This new element can describe 3-D deformations when the composite satisfies the assumption of GPS. To simulate the failure mode of interface, a kind of modified 2-D Goodman interface element, which is capable of describing 3-D failure mode, is constructed based on the RVE.

The experiments of soil-root composites were performed in Qinghai Province. Material parameters of soil and root were obtained by general experiments for the numerical simulation. The triaxial tests of soil-root composites were performed. The limit loads of axial pressure were obtained for different root fractions. The strength of soil was increased obviously with the increase of root fibers.

Limit loads of mental matrix composites was obtained based on the presented computational model and compared with literature on bonded and debonded interfaces. The soil and the soil-root composites were also calculated based on this model. The limit loads of soil-root composites were compared to the experiment results in triaxial tests. Good agreement of limit loads has been achieved between the numerical and the experimental results.

References

Aboudi, J. (1988): Constitutive equations for elastoplastic composites with imperfect bonding. *International Journal of Plasticity*, vol.4, pp. 103-125.

Aghdam, M.M.; Smith, D.J.; Pavier, M.J. (2000): Finite element micromechanical modeling of yield and collapse behavior of metal matrix composites, *Journal*

of Mechanics and Physics of Solids, vol.48, pp.499-528.

Benveniste,Y. (1985): The effective mechanical behaviour of composite materials with imperfect contact between constituents. *Mechanics of Materials*, vol.4, pp.197-208.

Buhan, P; Taliercio, A. (1991): A homogenization approach to the yield strength of composite materials, *European Journal of Mechanics, A /Solids*, vol.10, pp. 129-154.

Carvelli, V; Maier, G.; Taliercio A. (2000): Kinematic limit analysis of periodic heterogeneous media, *CMES: Computer Modeling in Engineering & Sciences*, vol. 1, pp. 19-30.

Desai, C.S.; Zaman, M.M.; Lightner, J.G.; Siriwardane, H.J. (1984): Thin-layer element for interfaces and joints. *International Journal for Numerical and Analytical Methods in Geomechanics*, vol.8, pp.19-43.

Gray, D.H.; Ohashi, H. (1983): Mechanics of fiber reinforcement in sand. *Journal of Geotechnical Engineering, ASCE*, vol.109, pp.335-353.

Goodman, R.E.; Taylor, R.L.; Brekke, T.L. (1968): A model for the mechanics of jointed rock. *Journal of the Soil Mechanics and Foundations Division, ASCE*, vol. 94, No. SM3, Mar.

Han, R.; Ingber, M.S.; Schreyer, H.L. (2006): Progression of failure in fiber-reinforced materials. *CMC: Computers Materials & Continua*, vol. 4, pp. 163-176.

Hashin, Z.; Shtrikman, S. (1962): On some variational principles in anisotropic and nonhomogeneous elasticity. *Journal of Mechanics and Physics of Solids*, vol.10, pp. 335-342.

Hill, R.(1965): A self-consistent mechanics of composite materials. *Journal of Mechanics and Physics of Solids*, vol.13, pp.213-222.

Litewka, A. (1980): Experimental study of the effective yield surface of perforated materials. *Nuclear Engineering and Design*, vol. 57, pp. 417-425.

Michel, J.C.; Mouline, H.; Suquet, P. (1999): Effective properties of composite materials with periodic microstructure: a computational approach. *Computer Methods in Applied Mechanics and Engineering*, vol. 172, pp. 109-132.

Michel, J.C.; Mouline, H.; Suquet, P. (2000): A computational method based on augmented Lagrangians and fast Fourier Transforms for composites with high contrast. *CMES: Computer Modeling in Engineering & Sciences*, vol. 1, pp. 79-88.

Mori, T.; Tanaka, K. (1973): Average stress in matrix and average elastic energy of materials with misfitting inclusions. *Acta Metallurgica*, vol.21, pp. 571-574.

Nilaweera, N.S.; Nutalaya, P. (1999): Role of tree roots in slope stabilization.

Bulletin of Engineering Geology and the Environment, vol.57, pp.337-342.

Operstein, V.; Frydman, S. (2000): The influence of vegetation on soil strength. *Ground Improvement*, vol.4, pp.81-89.

Okada, H.; Fukui, Y.; Kumazawa, N. (2004): Homogenization analysis for particulate composite materials using the boundary element method. *CMES: Computer Modeling in Engineering & Sciences*, vol. 5, pp. 135-149.

Pindera, M.J.; Aboudi, J. (1988): Micromechanical analysis of yielding of metal matrix composites. *International Journal of Plasticity*, vol.4, pp.195-214.

Sahchez-Palenciz, E. (1980): Nonhomogeneous media and vibration theory. *Lecture Notes in Physics*, vol.127, Springer-Verlag.

Suquet, P. (1987): *Homogenization Techniques for Composite Media*. Springer.

Taliercio, A. (2005): Generalized plane strain finite element model for the analysis of elastioplastic composites. *International Journal of Solids and Structures*, vol.42, pp. 2361-2379.

Teply, J.L.; Dvorak, G.J. (1988): Bounds on overall instantaneous properties of elastic-plastic composites. *Journal of the Mechanics and Physics of Solids*, vol.36, pp.29-58.

Waldon, L.J.; Dakessian, S. (1981): Soil reinforcement by roots: calculation of increased shear resistance from root properties. *Soil Science*, vol. 132, pp.427-435.

Waldon, L.J. (1977): The shear resistance of root-permeated homogeneous and stratified soil. *Journal of the Soil Science Society of America*, vol.41, pp.843-849.

Wu, T.H.; Beal, P.E.; Lan, C. (1988): In-situ shear tests of soil root system. *Journal of Geotechnical Engineering, ASCE*, vol.114, pp.1376-1394.

Wu, T.H.; McOmber, R.M.; Erb, R.T.; Beal, P.E. (1988): A study of soil root interaction. *Journal of Geotechnical Engineering, ASCE*, vol.114, pp.1351-1375.

Wu, T.H.; McKinnell, W.P.; Swanston, D.N. (1979): Strength of tree roots and landslides on Prince of Wales Island, Alaska, *Canadian Geotechnical Journal*, vol.16, pp.19-33.